

Expanding Catch and Release DNA Decoy (CRDD) Technology with Pyrimidine Mimics

Samantha A. Kennelly,^[a] Ramkumar Moorthy,^[a] Ruben Silva Otero,^[a] and Daniel A. Harki^{*[a]}

Abstract: Catch and release DNA decoys (CRDDs) utilize photochemically responsive nucleoside analogues that generate abasic sites upon exposure to light. Herein, we describe the synthesis and evaluation of four candidate CRDD monomers containing nucleobases that mimic endogenous pyrimidines: 2-nitroimidazole (**2-NI**), 2-nitrobenzene (**2-NB**), 2-nitropyrrole (**2-NP**) and 3-nitropyrrole (**3-NP**). Our studies reveal that **2-NI** and **2-NP** can function as CRDDs, whereas **3-NP** and **2-NB** undergo decomposition and transformation to

a higher-ordered structure upon photolysis, respectively. When incorporated into DNA, **2-NP** undergoes rapid photochemical cleavage of the anomeric bond (1.8 min half-life) to yield an abasic site. Finally, we find that all four pyrimidine mimics show significantly greater stability when base-paired against the previously reported 7-nitroindole CRDD monomer. Our work marks the expansion of CRDD technology to both purine and pyrimidine scaffolds.

Introduction

Caged oligonucleotides have been designed to target proteins and nucleic acids, allowing for the control of protein function or gene expression following photolysis of nucleotide monomers containing photolabile groups.^[1–3] These caged oligonucleotides (or caged DNA decoys for our application) are usually modulated in a temporal *off-to-on* manner.^[3–8] The turn-on mechanism of the synthetic oligonucleotides are due to the bulkiness of substituents (cages) on DNA bases that cannot form stable Watson-Crick-Franklin base pairs with cognate bases in a DNA duplex structure. Photolysis of the caged DNA decoy promotes a series of reactions to cleave the light-reactive substituents.^[1–10]

Caged DNA decoys have typically included a nitro-functionalized group (e.g., *ortho*-nitrobenzyl) as it possesses the ability to form a radical species upon photolysis that results in the formation of a native nucleotide.^[4–7,9,10] Caged DNA decoys have been applied to photoregulate a variety of biological processes including transcription, nucleic acid folding, polymerase activity, DNA repair, gene silencing, antisense activity, siRNA function, DNAzymes, and aptamer function.^[7,11–23]

An extension of caged DNA decoy technology has been the development of catch and release DNA decoys (CRDDs).^[20] Unlike caged DNA decoys that temporarily render biologically

active oligonucleotides inactive, CRDDs function in an *on-to-off* manner. CRDDs are initially competent to engage their biological target (the CRDD is *on*), but upon photolysis, the CRDD becomes inactivated (or turned *off*). Notably, elegant work by others have utilized photolabile protecting groups to develop *on-to-off* controllable systems for various oligonucleotide applications (e.g., RNA bandages,^[24] DNAzymes,^[18,25] triplex-forming oligonucleotides,^[26] and antisense oligonucleotides^[18]), although such *on-to-off* platforms are much less common. The utility of CRDDs over caged DNA decoys lies in their orthogonal temporal control of DNA decoy function. Previous work targeted the NF- κ B p50-p65 heterodimer with CRDDs containing the universal base 7-nitroindole (**7-NI**) in the nucleotide monomer (Figure 1A)^[20] Established CRDD technology utilizes single-photon UV-irradiation to cleave the anomeric bond, leading to depurination between the sugar and nucleobase to achieve inactivation of the DNA decoy and its binding to NF- κ B proteins (Figure 1A). The photoproducts of **7-NI** photolysis have been previously characterized to be the abasic 2'-deoxyribose sugar and the 7-nitrosoindole base.^[27–29] Herein, we expand the repertoire of monomers to include pyrimidine mimics and complete the toolbox of depurination competent monomers for CRDD technology. Accordingly, we report that 2-nitropyrrole (**2-NP**) and 2-nitroimidazole (**2-NI**) nucleobases once incorporated into 2'-deoxynucleosides can function as next-generation, pyrimidine-mimicking CRDD monomers (Figure 1B).

Results and Discussion

Our studies commenced with two previously synthesized nucleoside analogues containing 2-nitropyrrole (**2-NP**) and 3-nitropyrrole (**3-NP**) nucleobases, whose photoproducts have not been characterized and usage as CRDDs have not been explored (Figure 2).^[30–37] In fact, both **2-NP** and **3-NP** were

[a] S. A. Kennelly, Dr. R. Moorthy, Dr. R. S. Otero, Prof. Dr. D. A. Harki
Department of Medicinal Chemistry
University of Minnesota
2231 6th Street SE, Minneapolis, MN 55455 (USA)
E-mail: daharki@umn.edu

Supporting information for this article is available on the WWW under <https://doi.org/10.1002/chem.202201355>

© 2022 The Authors. Chemistry - A European Journal published by Wiley-VCH GmbH. This is an open access article under the terms of the Creative Commons Attribution Non-Commercial NoDerivs License, which permits use and distribution in any medium, provided the original work is properly cited, the use is non-commercial and no modifications or adaptations are made.

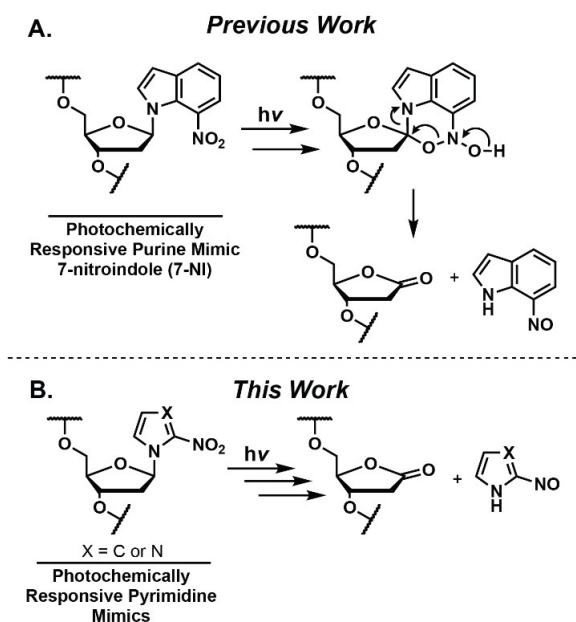


Figure 1. A) The previously reported 7-NI CRDD monomer that mimics purines. B) This work: expanding the chemical toolbox of CRDDs with photochemically responsive pyrimidine mimics that undergo photolysis to release a 2'-deoxyribose lactone and nitrosobase.

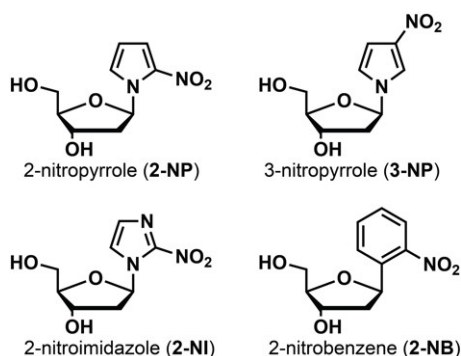
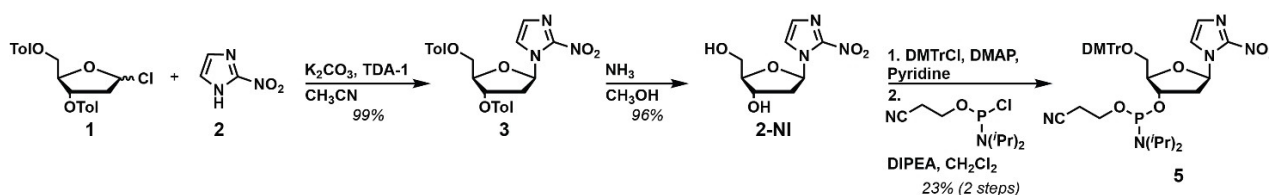


Figure 2. Pyrimidine nucleoside mimics used in this study.

designed to mimic the universal base *p*-nitroaniline, and thus possess enhanced stacking interactions and the ability to polarize the electrostatic potential of the π -aromatic pyrrole; a common feature of nitro-containing compounds.^[30–32,35] Additionally, 2-NP and 3-NP were previously characterized as



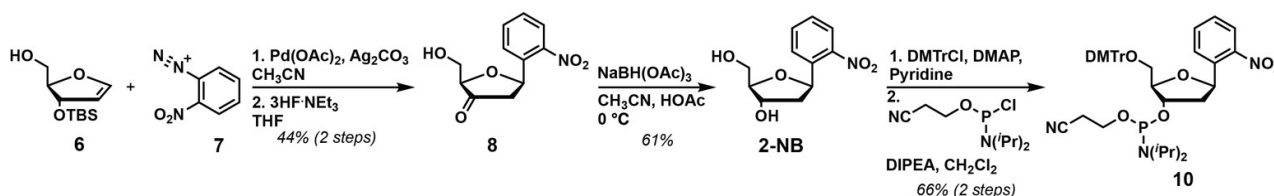
Scheme 1. Synthesis of 2-NI and phosphoramidite 5.

universal bases, as they possess the ability to base pair with all of the natural DNA bases equivalently.^[31,37]

We also designed and synthesized two novel pyrimidine nucleoside mimics containing 2-nitroimidazole (2-NI) and 2-nitrobenzene (2-NB) nucleobases (Figure 2). We hypothesized that 2-NI will take advantage of stacking interactions involved in pyrrole-containing compounds, as well as possess hydrogen-bond accepting capability through the additional nitrogen atom in the imidazole. We designed 2-NB to contain structural similarities to that of the endogenous pyrimidines by bearing a six-membered ring. We also decided to utilize 2-NB in our studies as it bears structural resemblance to the commonly reported ortho-nitrobenzyl caging group. Finally, this compound would also allow an evaluation of depurination potential through a C–C anomeric bond. Taken together, our study employs four scaffolds, 2-NP, 3-NP, 2-NI, and 2-NB to mimic the endogenous pyrimidine DNA bases and function as depurination-competent monomers suitable for utilization in CRDDs.

1-(2'-Deoxy-β-D-ribofuranosyl)-2-nitroimidazole (2-NI) was synthesized as shown in Scheme 1 by direct attachment of the protected furanose 1 to 2-nitroimidazole (2). 2-NI was generated in two steps from 1-chloro-2-deoxy-3,5-di-O-toluoyl-D-erythropentofuranose (1) and 2-nitroimidazole (2) by the addition of K_2CO_3 and phase transfer catalyst tris(2-(2-methoxyethoxy-ethyl)amine) (TDA-1), followed by the deprotection of the tolyl groups. For incorporation into oligonucleotides, the phosphoramidite of 2-NI, compound 5, was synthesized in two steps from 2-NI through the protection of the 5'-alcohol with dimethoxytrityl chloride followed by the addition of 2-cyanoethyl-*N,N*-diisopropylchlorophosphoramidite on the 3'-alcohol.

1-(2'-Deoxy-β-D-ribofuranosyl)-2-nitrobenzene (2-NB) was synthesized as shown in Scheme 2 by Heck coupling of 6 to 2-nitrobenzenediazonium (7).^[38,39] After the Heck coupling reaction, removal of the TBS-protecting group and tautomerization to the more stable ketone was achieved by the addition of 3HF·NEt₃ (8).^[39] The reduction of the newly formed ketone to a secondary alcohol was afforded, yielding 2-NB. For incorporation into oligonucleotides, the phosphoramidite of 2-NB, compound 10, was synthesized in two steps from 2-NB through the protection of the 5'-alcohol with dimethoxytrityl chloride followed by the addition of 2-cyanoethyl-*N,N*-diisopropylchlorophosphoramidite on the 3'-alcohol. Finally, 1-(2'-deoxy-β-D-ribofuranosyl)-3-nitropyrrole (3-NP) and 1-(2'-deoxy-β-D-ribofuranosyl)-2-nitropyrrole (2-NP) were synthesized according to previous reports.^[33,37]



Scheme 2. Synthesis of the phosphoramidite of 2-NB.

The nucleoside analogues were first evaluated to determine if depurination occurs upon photolysis. The proposed mechanism for depurination was reported previously for related compounds,^[28,40–42] and therefore, we hypothesize that our compounds will also undergo a similar mechanism of depurination (Figures 3A and 4A; Scheme S1 in the Supporting Information). Photolysis studies were conducted at 254 or 350 nm according to the maximum absorbance values of the analogues under investigation (Figure S1). Typical depurination experiments were performed between 0.5–1.0 mM of the respective nucleoside in D₂O. Experiments were performed in a quartz cuvette and sample irradiation took place in a Rayonet holding either eight 254-nm or 350-nm bulbs depending on the maximum absorbance value of the nucleoside as previously discussed. Samples were then photolyzed at various time intervals (i.e., 0, 1, 2, 5, 10, 12, 14, 16, 18, 20, 30, and 60 min)

and the solution was characterized by high-performance liquid chromatography (HPLC) analysis, UV-vis and NMR spectroscopy.

UV-vis spectroscopy studies on 2-NP demonstrated a shift in the maximum absorbance upon prolonged light exposure (Figure 3B). A decrease in the maximum absorbance at 350 nm was initially observed after 5 min of photolysis, followed by the appearance of a blue-shifted absorbance around 215 nm after 10 min of photolysis. This blue-shifted absorbance was expected for 2-NP if photolysis yields 2'-deoxyribolactone, which possesses a maximum absorbance at 215 nm. The nitroso bases are not stable and volatile; thus they are not observed in our characterization studies. In order to characterize the kinetics of depurination, HPLC analysis was utilized. To quantify the nucleoside concentration (i.e., nucleoside remaining and depurinated product formed) throughout the time-course studies, the peak area was integrated. The percentage of formed depurination product was taken as a function over time for 2-

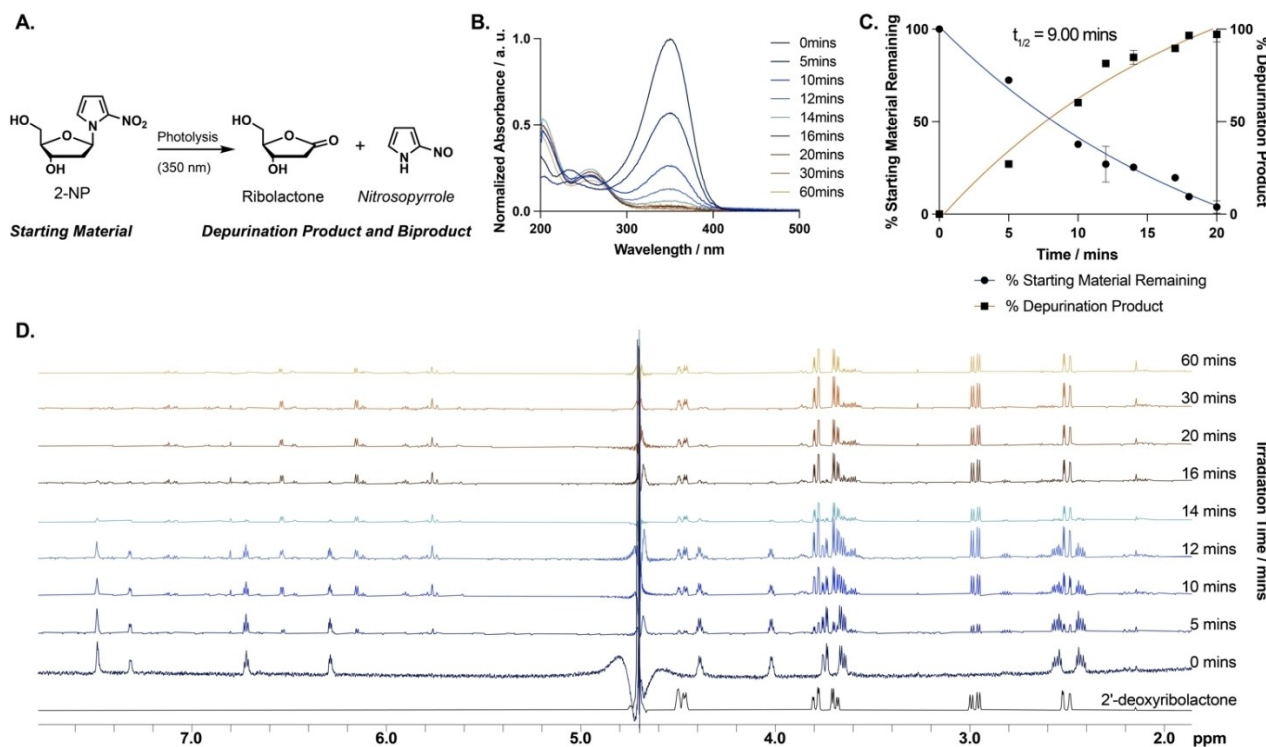


Figure 3. A) Characterization of 2-NP depurination. B) UV-vis spectroscopy illustrates a shift in the maximum absorbance of 2-NP from 350 nm at 0 min to 215 nm over 60 min. C) HPLC analysis shows the kinetics of 2-NP depurination; mean \pm SD ($n=3$). D) NMR spectroscopy demonstrates the depurination of 2-NP after photolysis.

NP (Figure 3C). The half-life ($t_{1/2}$) was calculated using one phase dissociation exponential decay for all compounds. **2-NP** formed depurination products most rapidly, with a $t_{1/2}$ of 9.00 min. Finally, NMR spectroscopy was performed on a Bruker 600 MHz Avance NEO equipped with a 5-mm triple resonance cryoprobe. These experiments yielded structural information on nucleoside depurination or nucleoside decomposition over the photolysis time, as well as confirmed that our compounds are indeed forming the anticipated depurination products. Therefore, 2'-deoxyribolactone was used as a standard in NMR studies to confirm whether the proposed depurination reaction was occurring. Observation of 2'-deoxyribolactone formation was apparent with **2-NP** as soon as 5 min upon initiation of photolysis; which was confirmed by complimentary UV-vis spectroscopy and HPLC analysis (Figure 3D). Complete consumption of starting material was observed after 20 min of photolysis for **2-NP**. From all three analytical characterization methods, we confirmed that **2-NP** does indeed undergo the intended depurination mechanism upon photolysis.

For **2-NI**, a similar trend in UV-vis spectroscopy studies was observed: after only 5 min of photolysis, the maximum absorbance at 325 nm decreased and a new blue-shifted absorbance peak was observed around 215 nm (Figure 4B). Once again, the blue-shifted peak was expected if 2'-deoxyribolactone was forming. The kinetics of depurination for **2-NI** were measured through HPLC analysis, in which a $t_{1/2}$ of 36.50 min was calculated (Figure 4C). The rate of photolysis for

compound **2-NI** was determined to be three-times slower than **2-NP**, which is not ideal for use in biological studies. Lastly, through NMR characterization, we confirmed the formation of 2'-deoxyribolactone after 10 min, which was confirmed by UV-vis spectroscopy and HPLC analysis (Figure 4D). Complete consumption of starting material was observed after 60 min for **2-NI**, which is much slower than **2-NP**.

3-NP showed an overall decrease in absorbance from 0 to 240 min after photolysis using UV-vis spectroscopy, which is indicative of decomposition (Figure S2A and B). The percentage of starting material remaining for **3-NP** as measured by HPLC analysis, resulted in a calculated $t_{1/2}$ of 20.40 min (Figure S2C). However, NMR studies confirmed that **3-NP** is indeed decomposing upon photolysis (Figure S2D).

Interestingly, during photolysis studies a slight red-shift in the maximum absorbance was observed with **2-NB**, leading us to believe that a different product other than the 2'-deoxyribolactone may be forming (Figure S3A and B). We also observed a color change in **2-NB** upon photolysis from a clear solution ($t=0$ min), to a bright yellow ($t=5$ min), and finally a brown solution ($t=240$ min), as well as the appearance of a precipitate (Figure S4B). In order to investigate the photolysis of **2-NB**, dynamic light scattering (DLS) was performed, as we believed that a larger molecular weight structure was forming due to the drastic changes in color and precipitate formation. DLS confirmed that a small molecule was detected at $t=0$ min, whereas at $t=60$ and 480 min, a polymeric material had formed

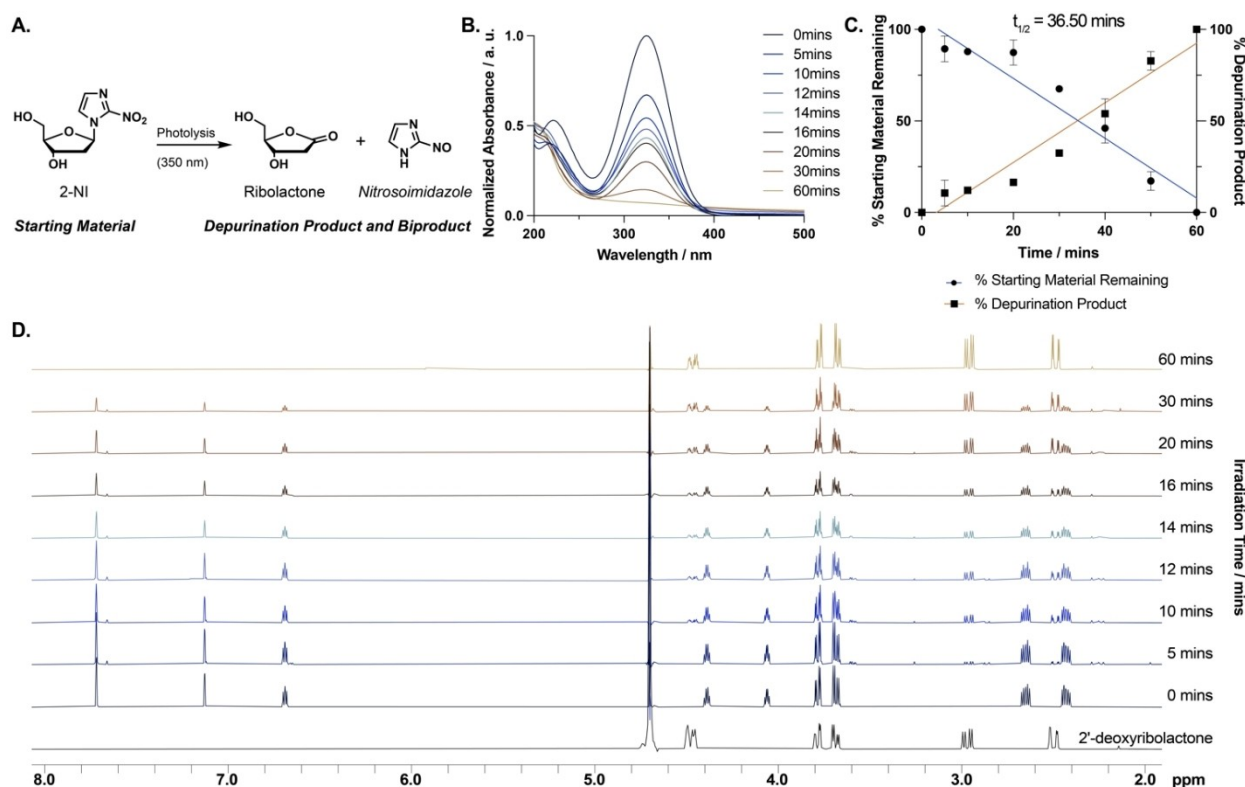


Figure 4. A) Characterization of **2-NI** depurination. B) UV-vis spectroscopy illustrates a shift in the maximum absorbance of **2-NI** from 325 nm at 0 min to 215 nm over 60 min. C) HPLC analysis shows the kinetics of **2-NI** depurination; mean \pm SD ($n=3$). D) NMR spectroscopy demonstrates the depurination of **2-NI** after photolysis. Mean \pm SD ($n=3$).

(Figure S4A). The percentage of starting material remaining was characterized for **2-NB**, which undergoes rapid transformation upon photolysis (Figure S3C). NMR studies confirmed starting material transformation to a higher-ordered structure within 1-min post photolysis of **2-NB** (Figure S3D).

From these initial UV-vis and NMR studies on our nucleoside analogues, we concluded that **2-NP** and **2-NI** form the desired photoproducts, whereas **3-NP** decomposes and **2-NB** transforms to a higher-ordered structure. Overall, it can be concluded from these quantitative HPLC studies that of the compounds that undergo depurination, **2-NP** and **2-NI**, the $t_{1/2}$ of **2-NP** is faster (9.00 min) as compared to **2-NI** (36.50 min). An ideal photocaging group will undergo photolysis rapidly, therefore, only **2-NP** will be taken forward for additional study.

Two control experiments were performed to determine the thermal- and photo-stability of the nucleoside mimics. A thermal stability study was performed to rule out thermal depurination of the nucleosides, as well as elucidate their thermal stability for future cellular studies (i.e., at 37 °C). The photo-stability study was accomplished to determine if photochemical depurination continues to occur outside of the Rayonet. From the thermal stability study, we determined that no significant change was observed in the maximum absorbance signal for all our analogues (Figure S5), thus confirming that heat produced from the Rayonet does not play a role in product decomposition, transformation to a higher-ordered structure, or depurination. Similarly, a photolysis stability study was performed on **2-NP** and **2-NI** to determine whether depurination continues to occur in the dark. UV-vis spectroscopy and HPLC analysis confirmed no significant loss of starting material over the experiment-time. We conclude that our nucleoside mimics are undergoing photo-induced depurination as anticipated (Figure S6).

After confirming that **2-NP** and **2-NI** undergo depurination and are stable when exposed to heat, we next sought to determine the stability of our analogues when incorporated into duplex DNA using a classical thermal melting temperature study (Table S1). Such studies yield important data to reveal which endogenous DNA base is most stable when paired against a particular pyrimidine mimic. Ultimately, data from this study will guide our designs containing these depurination-competent mimics. **3-NP** and **7-NI** were included as they could inform future applications of these universal bases.^[27,28,30–36]

Thermal melting curves confirmed that **2-NP**, **2-NI**, **3-NP**, **2-NB**, and **7-NI** are indeed universal bases (Table S1). This conclusion is supported by their ability to base pair with all of the natural bases with little discrimination. To our surprise, **2-NI** was the least stable, likely due to the increase in electronics from the additional nitrogen atom at the 3-position. Interestingly, all of the pyrimidine mimics showed slightly increased stability when base-paired with the endogenous purines adenine and guanine, which suggests that our compounds mimic endogenous pyrimidines. Excitingly, we found that **3-NP** and **2-NP**, as well as our novel analogues **2-NI** and **2-NB**, showed increased stability when base-paired against **7-NI** (Figure 5). In fact, the stability of these compounds when base-paired against **7-NI** was increased in comparison to adenine

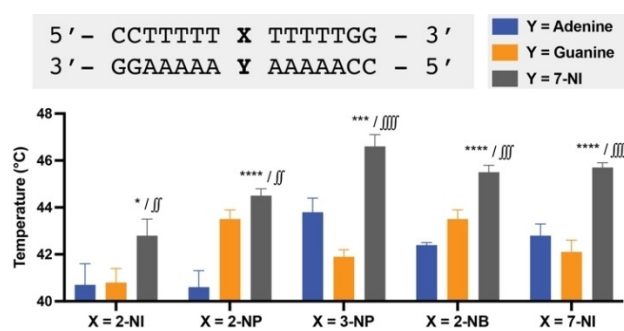


Figure 5. Thermal stability of the CRDD pyrimidine mimics when paired against the CRDD purine mimic **7-NI** in comparison to endogenous bases adenine (*) and guanine (j). An unpaired *t*-test in GraphPad Prism v9.3.1 was performed on the data shown in Table S1; */j denote $p < 0.05$, **/j denote $p < 0.01$, ***/j denote $p < 0.001$, and ****/j denote $p < 0.0001$; mean \pm SD ($n = 4$).

and guanine (Figure 5). Additionally, our pyrimidine analogues also displayed increased stability when base-paired against **7-NI** in comparison to the endogenous pyrimidine bases thymine and cytosine (Figure S7). To confirm that the structure of the DNA duplexes containing the depurinating pyrimidine mimics **2-NP** and **2-NI**, as well as the universal base **3-NP** are behaving similarly to natural base pairs, circular dichroism (CD) spectroscopy was performed (Figure 6A). CD characterization revealed that when **2-NP** and **2-NI** are separately base-paired against 2'-deoxyguanosine in a DNA duplex, they behave like a C–G base-pair (Figure 6A). Similarly, the secondary structure remained unchanged when the analogues were base-paired against **7-NI** in which they form DNA duplexes more stable than endogenous nucleotides due to hydrophobic interactions (Figure S7).

We determined that both **2-NP** and **2-NI** undergo the desired depurination mechanism to form the abasic 2'-deoxyribolactone; and thus have the ability to function as a CRDD. However, based on the unfavorable photolysis $t_{1/2}$ and decreased thermal stability of the nucleoside and oligonucleotide containing **2-NI**, respectively, we will focus our attention on **2-NP** for its use as a CRDD. DNA photolysis studies were conducted to define the kinetics of **2-NP** depurination in a duplex DNA (Figure 6B). In these studies, we used liquid chromatography-mass spectrometry (LC–MS) analysis of the irradiated aqueous sample **2-NP** base-paired against 2'-deoxyguanosine, as this base was found to be the most stable in our thermal stability studies (Figure S8; Table S1). Irradiation of the duplex DNA containing **2-NP** yields rapid photolysis ($t_{1/2} = 1.8$ min; 350 nm light; light intensity = 1.96×10^{-8} ein $\text{cm}^{-2}\text{s}^{-1}$), showing 71% of duplex being converted to photoproducts within 25 min (Figure 6C). In fact, very little **2-NP** remained after 25 min of irradiation, resulting in the formation of abasic sites and truncated β - and δ -elimination products. Our results yield a similar trend observed with our previously reported **7-NI**, which had a reported DNA photolysis $t_{1/2}$ of 1.0 min.^[20] Additionally, the rapid $t_{1/2}$ of the oligonucleotide containing **2-NP** will be beneficial for future in cellulo experiments.

Once again, we used CD spectroscopy on the DNA decoy containing **2-NP** to determine if DNA secondary structure

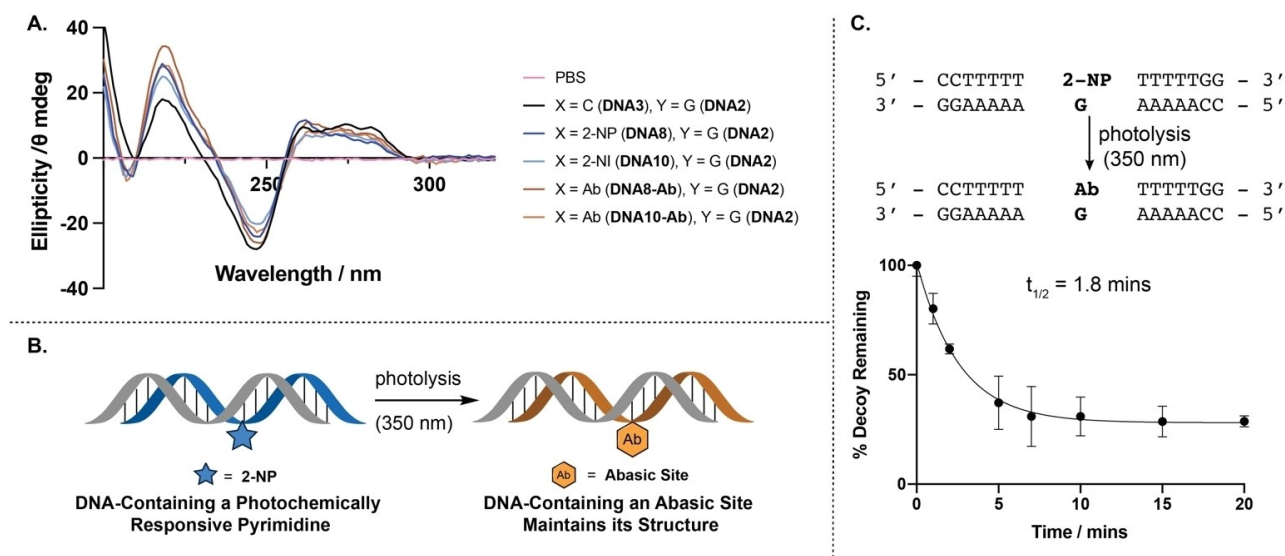


Figure 6. A) CD spectroscopy studies of oligonucleotides containing pyrimidines that depurinate upon photolysis. Experiments were performed in PBS buffer, pH 7.0, 25 °C, $N=2$ (see Table S3 for DNA sequences). B) Set-up of the 2-NP-containing DNA photolysis studies. C) Photolysis decay curve of a DNA duplex containing 2-NP with calculated half-life. Experiments were performed in aqueous 15 mM ammonium acetate; mean \pm SD ($n=3$).

remains intact after photolysis. We verified that DNA decoys containing 2-NP and 2-NI base-paired against 2'-deoxyguanosine in a double-stranded DNA duplex exhibited no change in secondary structure after photolysis (Figure S9). These experiments confirm that the structure of the DNA decoys containing a single CRDD monomer remains similar before and after photolysis, indicating the ability of DNA to bind to a target without disruption. Therefore, it is important to note that developing oligonucleotide sequences with multiple depurination sites for CRDD applications will be required to yield destabilized DNA for target disengagement, due to the formation of multiple abasic sites and DNA cleavage products. This trend was previously observed with CRDDs containing 7-NI,^[20] and is reminiscent of the requirement for incorporating multiple bulky, photolabile groups in caged DNA decoys,^[7] mRNA,^[43] microRNA,^[44] and siRNA,^[45] to block their biological functions.

Conclusion

Herein, we have expanded the chemical toolbox of photo-responsive CRDDs to pyrimidine-containing analogues. Through rigorous characterization of photoproducts, we determined that 2-NP and 2-NI undergo depurination, whereas 3-NP decomposes, and 2-NB transforms to a higher-ordered structure. Additionally, we discovered that photolysis of a duplex DNA containing 2-NP yields an abasic site at a rate similar to that of the CRDD purine predecessor 7-NI. Interestingly, we also revealed the increased stabilities of our pyrimidine mimics against 7-NI. We will use these findings in future studies by incorporating multiple 2-NP monomers into CRDDs for monitoring the dynamics of DNA-interacting proteins.

Experimental Section

General procedure: All commercial chemicals were used as received. Reactions were performed in flame-dried glassware under inert gas (N_2) and stirred using a Teflon-coated magnetic stir bar. Reaction solvents acetonitrile (CH_3CN), dichloromethane (CH_2Cl_2), and tetrahydrofuran (THF) were dried by passage over a column of activated alumina using a solvent purification system (MBraun). *N,N*-Diisopropylethylamine (DIPEA) was vacuum distilled from calcium hydride and placed under argon with 4 Å molecular sieves. 2-nitroimidazole was obtained from Accela. 3-Nitro-1*H*-pyrrole was obtained from LabNetwork. 3-Nitropyrrole-2'-deoxynucleoside was obtained from Berry & Associates. 2-Nitro-1*H*-pyrrole was obtained from BLD Pharmtech. Tris(2-(2-methoxyethoxy-ethyl)amine (TDA-1) was obtained from TCI. 4-dimethylaminopyridine was obtained from Oakwood Chemicals. 2-deoxy-D-ribose and 3,5-di-O-toluyl- α -1-chloro-2-deoxy-D-ribofuranose (**1**) were obtained from Carbosynth. All other general reagents were obtained from either Acros, Alfa Aesar, or Sigma Aldrich. Reactions were monitored using EMD Chemicals Silica Gel 60 F₂₅₄ glass plates (250 μ m thickness) and visualized with UV irradiation at either 254 or 365 nm. Silica gel chromatography was accomplished using a Teledyne-Isco Combi-flash Rf-200 instrument using Redisep Rf High-Performance silica gel columns from Teledyne-Isco. ¹H NMR (600 MHz) and ¹³C (151 MHz) were collected on a Bruker 600-MHz Avance NEO equipped with a 5-mm triple resonance cryoprobe at room temperature (at the Minnesota NMR Center). A Bruker 500-MHz Avance NMR spectrometer was used to collect ³¹P NMR (202 MHz) at room temperature. The ¹³C NMR spectrum in D₂O were referenced through the solvent lock (²H) signal according to the IUPAC recommended secondary referencing method. High resolution mass spectra were obtained at the Analytical Biochemistry Core Facility at the University of Minnesota Masonic Cancer Center using an LTP Orbitrap Velos Mass Spectrometer (Thermo Fisher).

1-(2'-Deoxy-3',5'-di-O-toluoyl- β -D-ribofuranosyl)-2-nitroimidazole (3): 2-Nitroimidazole (**2**) (1.01 g, 8.84 mmol), potassium carbonate (4.03 g, 29.2 mmol), and tris(2-(2-methoxyethoxy-ethyl)amine (TDA-1; 56.5 μ L, 0.176 mmol) were dissolved in anhydrous acetonitrile (50 mL) and stirred for one hour at room temperature before the

addition of 3,5-di-*O*-toluyl- α -1-chloro-2-deoxy-D-ribofuranose (1; 3.89 g, 11.5 mmol) in small portions. The mixture was stirred further for 2 h at room temperature. After the completion of the reaction (monitored by TLC), the reaction mixture was filtered over celite and washed with Et₂O (30 mL). The filtrate was concentrated in vacuo and the crude material was purified by flash column chromatography on SiO₂ (gradient 1–2% acetone in CH₂Cl₂) yielding 4.07 g (99%) of **3** as a white foam. ¹H NMR (600 MHz, CDCl₃): δ = 7.95 (d, *J* = 8.3 Hz, 2H), 7.84 (d, *J* = 8.3 Hz, 2H), 7.58 (d, *J* = 1.2 Hz, 1H), 7.28 (d, *J* = 8.0 Hz, 2H), 7.23 (d, *J* = 8.0 Hz, 2H), 7.10 (d, *J* = 1.2 Hz, 1H), 6.81 (app t, *J* = 7.1 Hz, 1H), 5.63–5.60 (m, 1H), 4.80–4.65 (m, 3H), 3.12 (ddd, *J* = 14.4, 5.7, 2.6 Hz, 1H), 2.51–2.45 (m, 1H), 2.44 (s, 3H), 2.41 (s, 3H). ¹³C NMR (151 MHz, CDCl₃): δ = 166.2, 166.1, 144.8, 144.6, 144.0, 129.9 (2 C), 129.7 (2 C), 129.5 (2 C), 129.4 (2 C), 128.9, 126.5, 126.2, 121.7, 89.6, 84.1, 74.4, 63.8, 40.8, 21.8, 21.8. HRMS (ESI) *m/z*: calcd for C₂₄H₂₃N₃O₇Na: 488.1428 [*M* + Na]⁺; found 488.1414.

1-(2'-Deoxy- β -D-ribofuranosyl)-2-nitroimidazole (2-NI): Compound **3** (4.07 g, 8.75 mmol) was dissolved in methanol (50 mL), followed by the addition of 7 N methanolic ammonia (50 mL) and the reaction mixture was stirred for 18 h at room temperature. The solution was concentrated in vacuo, and the crude material was purified by SiO₂ chromatography (gradient of 0–20% CH₃OH in CH₂Cl₂) to afford 1.92 g (96%) of **2-NI** as a white foam. The β -anomer was confirmed on the basis of the characteristic apparent triplet for the 1'-proton observed at 6.77 ppm (*J* = 4.8 Hz) wherein the case of the α -anomer the *J* value should be between 1.5–2.0 Hz.^[46] Additionally, the 1'-carbon of the α -anomer appears at 100 ppm, which is not observed.^[46] ¹H NMR (600 MHz, D₂O): δ = 7.80 (d, *J* = 1.3 Hz, 1H), 7.21 (d, *J* = 1.3 Hz, 1H), 6.77 (app t, *J* = 4.8 Hz, 1H), 4.47 (app q, 5.7 Hz, 1H), 4.18–4.08 (m, 1H), 3.87 (dd, *J* = 12.6, 3.6 Hz, 1H), 3.77 (dd, *J* = 12.6, 5.5 Hz, 1H), 2.74 (ddd, *J* = 14.2, 6.5, 5.4 Hz, 1H), 2.51 (ddd, *J* = 14.2, 6.4, 5.1 Hz, 1H). Exchangeable protons (hydroxyls) are not observed since the compound NMR was obtained in D₂O. ¹³C NMR (151 MHz, D₂O): δ = 143.8, 127.8, 122.9, 88.5, 87.3, 69.7, 60.8, 40.6. HRMS (ESI) *m/z*: calcd for C₈H₁₂N₃O₅: 230.0777 [*M* + H]⁺; found 230.0767.

1-(2'-Deoxy-5'-dimethoxytrityl- β -D-ribofuranosyl)-2-nitroimidazole (4): Compound **2-NI** (150 mg, 0.655 mmol) was dissolved in anhydrous pyridine (1 mL) and the resulting solution was concentrated in vacuo. This process was repeated 3X to remove residual water from **2-NI**. The material was then dried over high-vacuum for 1 hr before the addition of 4,4'-dimethoxytrityl chloride (222 mg, 0.655 mmol) and 4-dimethylaminopyridine (8.00 mg, 0.0655 mmol), which was then dissolved in anhydrous pyridine (1.5 mL). The reaction mixture was allowed to stir overnight (18 h) at room temperature. The solution was concentrated in vacuo and the crude material was purified by flash column chromatography on neutralized SiO₂ (neutralized by washing with 2 column volumes of 1% Et₃N in CH₂Cl₂) using a gradient of 0–10% acetone in CH₂Cl₂ to yield 268 mg (77%) of **4** as a white foam. ¹H NMR (600 MHz, [D₆]DMSO): δ = 7.68 (s, 1H), 7.40–7.35 (m, 2H), 7.31 (t, *J* = 7.6 Hz, 2H), 7.28–7.20 (m, 5H), 7.10 (d, *J* = 1.1 Hz, 1H), 6.89 (d, *J* = 8.4 Hz, 4H), 6.59 (dd, *J* = 6.5, 4.2 Hz, 1H), 5.41 (d, *J* = 4.9 Hz, 1H), 4.31 (p, *J* = 6.0 Hz, 1H), 4.04–3.98 (m, 1H), 3.74 (s, 6H), 3.26 (dd, *J* = 10.7, 3.0 Hz, 1H), 3.21 (dd, *J* = 10.7, 5.5 Hz, 1H), 2.49–2.46 (m, 1H), 2.39 (ddd, *J* = 10.7, 4.2, 3.2 Hz, 1H). ¹³C NMR (151 MHz, DMSO-*d*₆): δ = 158.1 (2 C), 144.6, 144.1, 135.4, 135.3, 129.8 (4 C), 127.9 (2 C), 127.7 (2 C), 127.6, 126.8, 122.7, 113.2 (4 C), 88.2, 85.8, 85.7, 68.8, 62.7, 55.0 (2 C), 41.4. HRMS (ESI) *m/z*: calcd for C₂₉H₂₉N₃O₇Na: 554.1897 [*M* + Na]⁺; found 554.1897.

1-(2'-Deoxy-5'-dimethoxytrityl- β -D-ribofuranosyl)-2-nitroimidazole-3'-O-(2-cyanoethyl-N,N-diisopropylphosphoramidite) (5): Compound **4** (31.0 mg, 0.0583 mmol) was dissolved in anhydrous acetonitrile (1 mL) and the resulting solution was concentrated in vacuo. This process was repeated 3x to remove residual water from

compound **4**. The material was then placed under vacuum for 1 h before the addition of anhydrous CH₂Cl₂ (1 mL), freshly distilled *N,N*-diisopropylethylamine (56.0 μ L, 0.321 mmol), and 2-cyanoethyl *N,N*-diisopropylchlorophosphoramidite (20.0 μ L, 0.0881 mmol). The reaction mixture was stirred at room temperature for 90 min under N₂. The solution was concentrated in vacuo, and the crude material was purified by neutralized SiO₂ chromatography (neutralized by washing with 2 column volumes of 1% Et₃N in CH₂Cl₂ using a gradient 0–30% EtOAc in cyclohexanes to afford 12.0 mg (30%) of **5** as a white foam (a diastereomeric mixture). ¹H NMR (600 MHz, CDCl₃): δ = 7.72 (d, *J* = 1.2 Hz, 0.39H), 7.64 (d, *J* = 1.2 Hz, 0.61H), 7.40–7.33 (m, 2H), 7.30–7.16 (m, 7H), 6.96–6.90 (m, 1H), 6.83–6.74 (m, 4H), 6.67–6.61 (m, 1H), 4.66–4.60 (m, 0.37H), 4.60–4.54 (m, 0.64H), 4.23–4.17 (m, 1H), 3.87–3.77 (m, 1H), 3.75–3.73 (m, *J* = 3.7 Hz, 6H), 3.73–3.66 (m, 1H), 3.62–3.51 (m, 2H), 3.51–3.43 (m, 1H), 3.37–3.31 (m, 1H), 2.85–2.72 (m, 1H), 2.57 (t, *J* = 6.3 Hz, 1.2H), 2.40 (t, *J* = 6.4 Hz, 0.75H), 2.37–2.29 (m, 1H), 1.17–1.08 (m, 8H), 1.03 (d, *J* = 6.8 Hz, 4H). ¹³C NMR (151 MHz, CDCl₃): Major diastereomer δ 158.7, 144.3, 143.9, 135.3, 130.2 (2 C), 128.5 (2 C), 128.2, 128.0 (2 C), 127.1, 122.7, 117.4, 113.8 (4 C), 89.0, 86.9, 86.1, 86.0, 71.5, 71.4, 61.9, 58.4, 58.2, 55.3 (2 C), 43.4, 43.3, 42.1, 42.1, 24.7, 24.6 (2 C), 20.3, 20.2. Minor diastereomer δ 158.7, 144.2, 143.9, 135.4, 130.2 (2 C), 128.4 (2 C), 128.3, 128.0 (2 C), 127.2, 122.6, 117.5, 113.8 (4 C), 89.0, 86.8, 85.9, 85.9, 72.1, 72.0, 62.0, 58.2, 58.1, 55.3 (2 C), 43.3, 43.3, 42.3, 42.3, 24.6, 24.6 (2 C), 20.4, 20.4. ³¹P NMR (202 MHz, CDCl₃): δ = 149.52, 148.98. HRMS (ESI) *m/z*: calcd for C₃₈H₄₇N₅O₈P: 732.3162 [*M* + H]⁺; found 732.3136.

3-O-(tert-Butyldimethylsilyl)-1,2-didehydro-1,2-dideoxy-D-ribofuranose (6): The synthesis of 3-O-(tert-butyldimethylsilyl)-1,2-didehydro-1,2-dideoxy-D-ribofuranose was prepared as previously described from the commercially available 2-deoxy-D-ribose in four steps.^[39]

2-Nitrobenzenediazonium (7): The synthesis of 2-nitrobenzenediazonium was prepared as previously described from the commercially available 2-nitroaniline in one step.^[38]

1-(2'-Deoxy-3'-oxo- β -D-ribofuranosyl)-2-nitrobenzene (8): Freshly prepared **6**^[39] (1.38 g, 5.99 mmol) and **7**^[38] (1.71 g, 7.19 mmol) were placed in two separate flasks under argon and were dissolved in degassed CH₃CN (5 mL). In a separate Schlenk flask under N₂, palladium acetate (0.269 g, 1.20 mmol) with silver carbonate (1.66 g, 6.01 mmol) were added. Next, the complete addition of the fully dissolved **6**, and then followed by the complete addition of dissolved **8** were added to the reaction mixture in the Schlenk flask. The reaction mixture was stirred for 2 h. The solution was then filtered over a short pad of silica gel and washed with ethyl acetate (50 mL). The filtrate was concentrated in vacuo to yield crude material which was then re-dissolved in THF (40 mL), followed by the addition of triethylamine trihydrofluoride (0.98 mL, 6.01 mmol). The reaction mixture was stirred at room temperature, showing complete conversion by TLC in 30 min. The solution was concentrated in vacuo, and the crude product was purified by SiO₂ chromatography (gradient 0–20% CH₃OH in CH₂Cl₂) to afford 0.632 g (44%) of **9** as a dark red liquid (as a 10:1 mixture of **9** and its anomer which was removed during a later step in the synthesis). ¹H NMR (600 MHz, CDCl₃): δ = 8.06 (d, *J* = 8.2 Hz, 2H), 7.73 (t, *J* = 7.7 Hz, 1H), 7.51 (t, *J* = 7.8 Hz, 1H), 5.75 (dd, *J* = 10.6, 5.9 Hz, 1H), 4.11 (app t, *J* = 3.5 Hz, 1H), 4.04 (dd, *J* = 6.2, 3.5 Hz, 2H), 3.28 (dd, *J* = 18.4, 5.9 Hz, 1H), 2.43–2.32 (m, 1H), 1.94 (app t, *J* = 6.3 Hz, 1H). ¹³C NMR (151 MHz, CDCl₃): δ = 213.0, 147.6, 136.6, 134.4, 129.0, 127.5, 124.8, 82.1, 73.8, 61.7, 45.4. HRMS (ESI) *m/z*: calcd for C₁₁H₁₂NO₅: 238.0715 [*M* + H]⁺; found 238.0704.

1-(2'-Deoxy- β -D-ribofuranosyl)-2-nitrobenzene (2-NB): Compound **8** (0.632 g, 2.66 mmol) was dissolved in a 1:1 mixture of CH₃CN:AcOH (20 mL solution) and cooled to 0°C. NaBH(OAc)₃ (0.850 g,

3.99 mmol) was then added to the solution and was stirred for 90 min at 0 °C before quenching by the addition of methanol (5 mL). The solution was concentrated in vacuo, and the crude material was purified by SiO₂ chromatography (gradient 0–20% CH₃OH in CH₂Cl₂) to afford 0.388 g (61%) of **2-NB** as a white foam. The β -anomer was confirmed on the basis of the characteristic doublet of doublets (dd) for the 1'-proton observed at 5.68 ppm ($J=10.0$ and 5.8 Hz) and the narrow multiplet (0.1 ppm width) observed for the two 2' protons, wherein the case of the α -anomer the J value should be between 1.5–2.0 Hz. Additionally, the 1'-carbon of the α -anomer appears at 100 ppm, which is not observed.^[46,47] ¹H NMR (600 MHz, D₂O): $\delta=8.07$ (d, $J=8.2$ Hz, 1H), 7.91 (d, $J=8.0$ Hz, 1H), 7.80–7.75 (m, 1H), 7.58–7.53 (m, 1H), 5.68 (dd, $J=10.0, 5.8$ Hz, 1H), 4.36–4.31 (m, 1H), 4.03–3.97 (m, 1H), 3.75 (dd, $J=12.1, 4.5$ Hz, 1H), 3.71 (dd, $J=12.2, 5.9$ Hz, 1H), 2.60 (ddd, $J=13.7, 5.8, 2.2$ Hz, 1H), 2.07 (ddd, $J=13.7, 10.0, 6.1$ Hz, 1H). Exchangeable protons (hydroxyls) are not observed as compound NMR was obtained in D₂O. ¹³C NMR (151 MHz, D₂O): $\delta=147.2, 136.7, 134.3, 128.6, 127.2, 124.6, 86.8, 76.2, 72.5, 61.9, 41.9$. HRMS (ESI) m/z : calcd for C₁₁H₁₄N₃O₅: 240.0872 [$M+H$]⁺; found 240.0861.

1-(2'-Deoxy-5'-dimethoxytrityl- β -D-ribofuranosyl)-2-nitrobenzene (9): Compound **2-NB** (0.150 g, 0.512 mmol) was dissolved in anhydrous pyridine (1 mL) and the resulting solution was concentrated in vacuo. This process was repeated 3x to remove residual water from compound **2-NB**. The material was then placed under vacuum for 1 h before the addition of 4,4'-dimethoxytrityl chloride (0.221 g, 0.512 mmol) and 4-dimethylaminopyridine (7.90 mg, 0.0512 mmol), which was dissolved in anhydrous pyridine (1.5 mL). The solution was stirred at room temperature overnight (18 h). The solution was concentrated in vacuo and the crude material was purified by flash column chromatography on neutralized SiO₂ (neutralized by washing with 2 column volumes of 1% Et₃N in CH₂Cl₂) using a gradient of 0–10% acetone in CH₂Cl₂ to afford 0.300 g (88%) of **9** as a white foam. ¹H NMR (600 MHz, CDCl₃): $\delta=7.91$ –7.85 (m, 2H), 7.49–7.43 (m, 1H), 7.41–7.36 (m, 2H), 7.36–7.30 (m, 1H), 7.30–7.25 (m, 4H), 7.25–7.08 (m, 4H), 6.78–6.71 (m, 4H), 5.58 (dd, $J=8.9, 6.3$ Hz, 1H), 4.31 (quint, $J=6.8$ Hz, 1H), 3.98 (app q, $J=4.4$ Hz, 1H), 3.70 (s, 6H), 3.36–3.27 (m, 2H), 2.52 (ddd, $J=13.3, 6.3, 3.2$ Hz, 1H), 1.92 (ddd, $J=13.3, 8.9, 6.5$ Hz, 1H). ¹³C NMR (151 MHz, CDCl₃): $\delta=158.8$ (2 C), 147.7, 145.1, 139.0, 136.2, 133.9, 130.4 (2 C), 130.4 (2 C), 128.5 (2 C), 128.3 (2 C), 128.2 (2 C), 128.1, 127.2, 124.7, 113.5 (4 C), 86.7, 85.9, 76.2, 74.2, 64.2, 55.5 (2 C), 43.7. HRMS (ESI) m/z : calcd for C₃₂H₃₂N₂O₇: 542.2179 [$M+H$]⁺; found 542.2183.

1-(2'-Deoxy-5'-dimethoxytrityl- β -D-ribofuranosyl)-2-nitrobenzene-3'-O-(2-cyanoethyl-N,N-diisopropylphosphoramidite) (10): Compound **9** (0.043 g, 0.080 mmol) was dissolved in CH₃CN (1 mL), and the resulting solution was concentrated in vacuo. This process was repeated 3x to remove residual water from **10**. The material was then placed under vacuum to dry for 1 h before the addition of CH₂Cl₂ (4 mL), freshly distilled DIPEA (75.7 μ L, 0.437 mmol), and 2-cyanoethyl *N,N*-diisopropylchlorophosphoramidite (35.3 μ L, 0.119 mmol) were added and stirred at room temperature for 90 min. The solution was concentrated in vacuo and the crude material was purified by neutralized SiO₂ chromatography (neutralized by washing with 2 column volumes of 1% Et₃N in CH₂Cl₂) using 30% EtOAc in cyclohexane to afford 44 mg (75%) of **10** as a white foam (as a diastereomeric mixture). ¹H NMR (600 MHz, CDCl₃): $\delta=8.04$ (d, $J=8.0$ Hz, 0.52H), 8.02–7.95 (m, 1.4H), 7.60–7.52 (m, 1H), 7.51–7.44 (m, 2H), 7.44–7.39 (m, 1H), 7.39–7.33 (m, 4H), 7.32–7.27 (m, 2H), 7.25–7.18 (m, 1H), 6.89–6.76 (m, 4H), 5.71–5.62 (m, 0.56H), 4.51–4.46 (m, 0.52H), 4.25–4.19 (m, 1H), 3.90–3.81 (m, 2H), 3.82–3.77 (m, 6H), 3.72–3.51 (m, 3H), 3.45 (dd, $J=10.1, 3.8$ Hz, 0.56H), 3.39 (dd, $J=10.1, 3.9$ Hz, 0.56H), 3.33 (ddd, $J=10.0, 8.8, 4.4$ Hz, 1H), 2.80–2.74 (m, 0.56H), 2.70 (ddd, $J=13.1, 6.1, 2.8$ Hz, 0.57H), 2.65 (t, $J=6.4$ Hz, 1H), 2.47–2.40 (m, 1H), 2.04–1.91 (m, 1H), 1.18 (d, $J=6.8$ Hz, 9H),

1.07 (d, $J=6.8$ Hz, 3H). ¹³C NMR (151 MHz, CDCl₃): Major diastereomer: $\delta=158.6, 147.7, 144.9, 138.7, 136.1, 136.1, 133.8, 130.2$ (2 C), 130.3, 128.4, 128.0, 127.9 (2 C), 126.9, 124.5, 117.8, 113.2 (4 C), 86.3, 85.5, 85.5, 76.3, 75.5, 75.3, 63.9, 58.6, 58.5, 55.3, 43.4, 43.3, 42.7, 42.7, 24.7 (2 C), 24.6, 24.6, 20.5, 20.5. Minor diastereomer: $\delta=158.6, 147.6, 144.9, 138.5, 136.0, 136.0, 133.7, 130.2$ (2 C), 130.3, 128.3, 128.0, 127.9 (2 C), 126.9, 124.4, 117.6, 113.2 (4 C), 86.3, 85.5, 85.5, 76.3, 75.2, 75.0, 63.5, 58.3, 58.2, 55.3, 43.4, 43.3, 42.9, 42.9, 24.7 (2 C), 24.6, 24.5, 20.3, 20.2. ³¹P NMR (202 MHz, CDCl₃): $\delta=148.7, 147.8$. HRMS (ESI) m/z : calcd for C₄₁H₄₉N₃O₈P: 742.3257 [$M+H$]⁺; found 742.3224.

Solid-phase DNA synthesis: Oligonucleotides were synthesized using standard solid-phase synthesis methods on the BioAutomation MerMade8 DNA/RNA synthesizer.^[20] The phosphoramidites of 2-nitroimidazole and 2-nitrobenzene were synthesized as described above. The phosphoramidite of 7-nitroindole was prepared as reported.^[20] All other phosphoramidites and reagents were purchased from Glen Research Corporation. Synthesis of all modified oligonucleotides were performed on a standard dG-CPG solid support (1.0 μ mol scale), purchased from Glen Research Corporation. Modified phosphoramidites were freshly prepared and dried under high vacuum for 1 h prior to utilization. Similarly, reagents were freshly placed on the synthesizer prior to synthesis. Molecular trap packs (166-100109, Biolytic) were added to the anhydrous acetonitrile (40-4050-50, Glen Research) and activator (30-3140-57, Glen Research) solutions. The factory method (BioAutomation) for standard DNA-couplings was utilized. However, the method was paused immediately prior to the incorporation of the modified phosphoramidite for off-system coupling. The off-system coupling was achieved by first removing the solid support from the synthesizer. The modified phosphoramidite (20.0 mg) was then dissolved in anhydrous acetonitrile (200.0 μ L) and taken up into a syringe (1 mL) and attached to one side of the solid support. A second syringe (1 mL) was loaded with activator (600.0 μ L) solution and attached to the other side of the solid support. With both pre-loaded syringes attached to the solid support, the solutions were mixed through the column, starting with the addition of the activator solution. The solutions were manually mixed through the solid support using the two syringes for a total of 20 min. After the 20-min mixing period, the solid support column was drained and washed with anhydrous acetonitrile (1 mL) and returned to the synthesizer for the remaining on-system phosphoramidite couplings. Following the synthesis of **DNA8-DNA13**, the resin was dried under a stream of N₂ for 1 h before being transferred to a glass fritted reaction vessel. For resin removal and deprotection, concentrated aqueous NH₄OH (2.5 mL) was added to the reaction vessel and the aluminum foil-covered vessel was placed in a shaker at room temperature for 18 h. After deprotection, the solution was filtered into two microcentrifuge tubes, and the fritted reaction vessel was rinsed with RNase/DNase free water (2 mL) and filtered into another microcentrifuge tube. The centrifuge tubes containing the synthesized DNA were placed in the –80 °C freezer until the solution was frozen. Once completely frozen, the centrifuge tubes were placed in a SpeedVac to evaporate off the ammonium hydroxide and RNase/DNase free water. Once a white powder was obtained (4 h), the synthesized DNA was dissolved in RNase/DNase free water, the tubes were combined, and the solution (~800 μ L) was purified by HPLC. After purification, the **DNA8-DNA13** were desalted with RNase/DNase free water using Illustra NAP-5 columns (Sephadex G-25 DNA grade, GE Healthcare) according to the manufacturer's instructions. The desalted oligonucleotides were quantified by UV-vis spectroscopy and confirmed by LC-MS.

HPLC purification and LC-MS analysis of DNA: Oligonucleotides were purified using previously described methods.^[20] Oligonucleotides were either synthesized following methods described or were

purchased from Integrated DNA Technologies (IDT) as desalted oligonucleotides and purity was checked by HPLC, as noted in Table S3.

Absorbance data and molar extinction coefficients of nucleoside analogues: UV-vis spectra were collected on an Agilent Cary 100 UV-vis spectrophotometer (using the Scan software, scanning from 200.0 to 500.0 nm with a spectral bandwidth (SBW) of 2.0 nm, and a source changeover at 400.0 nm) at 25.0 °C. Nucleosides were dissolved in distilled and deionized (dd)H₂O and placed in clean 10 mm path length quartz cuvettes (Starna Cells, Inc.). The maximum absorbance of each nucleoside analogue was measured in triplicate and normalized (Figure S1). The molar extinction coefficients of each analogue was measured using previously described methods,^[48] measured in triplicate in (dd)H₂O, and reported values were averaged (Figure S1).

Depurination studies of nucleoside analogues: Nucleoside and DNA photolysis experiments were carried out using a Rayonet photochemical reactor (RMR-600, Southern New England Ultraviolet Co.) fitted with either eight 350 or 254 nm bulbs. For nucleoside photolysis experiments, samples were prepared in a clean 10 mm path length quartz cuvette (Starna Cells, Inc.). Typical depurination experiments were done at concentrations ~1.0 mM, dissolving the nucleoside in D₂O from Cambridge Isotope Laboratories. The solution was transferred into a quartz cuvette fitted to a septum and placed in the Rayonet. Samples were then exposed to light at various time intervals (i.e., 0, 1, 5, 10, 15, 30, 60, 120, and 240 min) and quantitative analysis was determined by NMR, UV-vis, and HPLC spectroscopy, as previously described. Depurination studies on the nucleoside **3-NP** showed product decomposition (Figure S2A–D) while nucleoside **2-NB** showed transformation to a higher-ordered structure (Figure S3A–D).

NMR analysis of nucleoside photoproducts: A Bruker 600-MHz Avance NEO, equipped with a 5-mm triple resonance cryoprobe was used for structural determination of nucleosides for depurination studies at room temperature. Nucleosides for depurination studies were prepared as previously described. Aliquots (40 µL) of the ~1.0 mM solution in D₂O were taken at several time points (0, 1, 2, 5, 10, 12, 14, 16, 18, 20, 30, and 60 min) and placed directly into 3.0 mm NMR tubes for analysis. ¹H NMR experiments for all samples were taken and analyzed. The experiment was repeated to obtain a biological replicate (*n*=2 total analyses, analyzed using MestReNova).

UV-vis analysis of nucleoside photoproducts: An Agilent Cary 100 UV-vis spectrophotometer containing a six-cell, temperature-controlled block with a path length of 1 cm was used for monitoring changes in the maximum absorbance value of the nucleosides. Nucleosides for depurination studies were prepared as previously described. Aliquots (30 µL) of the ~1.0 mM solution were taken at several time points (0, 1, 2, 5, 10, 12, 14, 16, 18, 20, 30, and 60 min) and were diluted into 970 µL of ddH₂O which was placed into a clean 10 mm path length quartz cuvette (Starna Cells, Inc.). Data collection was done on the Cary WinUV Scan application, monitoring wavelengths from 200.0–500.0 nm with a source changeover at 400.0 nm. The experiment was repeated to obtain a biological replicate and technical replicate (*n*=3 total analyses). The average of the three sample runs were reported with SD.

HPLC analysis of nucleoside photoproducts: The kinetics of nucleoside depurination or decomposition were determined by HPLC analysis on an Agilent 1200 series instrument equipped with a diode array detector and a Zorbax SB-C3 column (5 µm, 300 Å, 0.5×150 mm, Agilent Technologies). The analysis method (0.8 mL/min flow rate) involved isocratic H₂O (98% H₂O; 2% CH₃CN; 0–5 min) followed by a linear gradient to 10% CH₃CN (5–10 min) and

finally a linear gradient of 10–90% CH₃CN (10–30 min). Wavelengths monitored=215 and 254 nm. Aliquots (50 µL) were taken at several time points (0, 1, 2, 5, 10, 12, 14, 16, 18, 20, 30, and 60 min) and dissolved in 100 µL of distilled and deionized H₂O. In order to determine the amount of nucleoside remaining and new product formation, the area under the chromatogram was integrated. The amount of nucleoside present at time 0 min was taken as 100%. The method was repeated to obtain a technical replicate. The experiment was repeated to obtain a biological replicate and technical replicate (*n*=4 total analyses). The average of the four sample runs were reported with SD.

Dynamic light scattering: DLS studies were performed on **2-NB**. DLS experiments were performed on a Punk instrument (Unchained Labs) in a 1 mL cuvette with a sample solution volume of 100 µL. Samples were prepared and photolyzed as previously mentioned. DLS results indicate that a small molecule is present at time 0 min, whereas at time 60 min a higher-ordered structure is observed and continues increasing in size with continued photolysis time, as observed at time 480 min (Figure S4A). Each sample run was averaged from 10 readings. The formation of a precipitate was visualized from lyophilized samples in which a dark solid was observed over photolysis time (Figure S4B).

Thermal stability studies of nucleoside analogues: The Rayonet produces heat at approximately 37.5 °C during photolysis studies. To rule out thermal depurination of nucleosides, samples were prepared as previously described and heated in a silicon oil bath at 40 °C (see Figure S5A for setup). UV-vis spectroscopy was used to analyze heated nucleoside samples as previously described. These data demonstrate that neither depurination nor product decomposition occur thermally.

Photolysis stability studies of nucleoside analogues: In order to determine if photochemical depurination continues to occur outside of the Rayonet, a control experiment was performed on **2-NI** and **2-NP**. Using the same sample preparation methods as previously described for photolysis experiments, samples were photolyzed for 15 min, and an aliquot of the sample was analyzed by HPLC. The sample solution was then kept in the refrigerator (4 °C) for 24 h before being reanalyzed. After 24 h, another aliquot was taken from the solution for HPLC analysis. No significant changes were observed in samples analyzed at time=0 min (first analysis) and 24 h (second analysis; Figure S6).

Characterization and purity assessment of DNA oligonucleotides: LC–MS was performed on an Agilent 1100 series HPLC instrument equipped with an Agilent MSD SL ion trap mass spectrometer (operating in negative ion mode). A Zorbax SB-C18 column (5 µm, 300 Å, 0.5×150 mm, Agilent Technologies) was used for LC–MS analysis. The analysis method (15 µL/min flow rate) involved 15 mM aqueous NH₄OAc containing 2% CH₃CN followed by a linear gradient of 2–25% CH₃CN (0–15 min) and 25–60% CH₃CN (15–25 min). Wavelength monitored=260 nm.

Thermal melting analysis of oligos: Thermal melting analyses were performed according to previously described methods and results are shown in Table S1.^[20] Mean *T_m* values (± SD) were calculated from the individual *T_m* values obtained from each replicate (*n*=4). We found that the previously characterized **3-NP** and **2-NP**, as well as our novel analogues **2-NI** and **2-NB**, showed significantly increased stability when base-paired against **7-NI** (Figure S7).

Depurination studies on DNA: The proposed mechanism of DNA depurination of the double-stranded DNA containing the **2-NP** oligonucleotide (**DNA8**) base-paired against 2'-deoxyguanosine (**DNA2**) reveals the abasic site (**DNA8-Abasic**) while **DNA2** remains intact after photolysis (Figure S8A). To enable quantitative analysis of photochemical decay of DNA decoys, calibration plots for each

DNA decoy were generated as previously described.^[20] Briefly, increasing concentrations of each DNA oligonucleotide (decoy and its most stable base-pair; 15.0, 23.0, 30.0, 45.0, 60.0, 90.0 pmol) were added to a fixed concentration of an unmodified DNA oligonucleotide (5'-TAACTA-3'; 100 pmol; **DNA7**) and analyzed by extracted ion current LC-MS (masses were monitored at the -4 charge state for decoys, and -2 charge state for the control). A calibration plot was created by plotting the ratio of **DNA8/DNA7** area under the curve versus DNA decoy concentration, yielding calibration plots with a slope-intercept equation of $R^2 > 0.96$ (Figure S8B). A simple linear regression analysis (GraphPad Prism, v9.3.1) was performed to obtain the calibration plot. Quantitative analysis of DNA decoy photolysis was performed by dissolving the DNA decoy (60.0 pmol) in 15 mM aqueous NH_4OAc and then adding the solution to conical pulled point vial inserts (250 μL ; Agilent, 8010-0125). Vessels containing the dsDNA (**DNA2** paired with **DNA7**) were placed into the photochemical reactor and irradiated (light intensity: 1.96×10^{-8} ein $\text{cm}^{-2} \text{s}^{-1}$). Aliquots (10 μL) were taken at several time points (0, 1, 2, 5, 7, 10, 15, 20, 25 min), diluted with standard (100 pmol, 1 μL), and then analyzed by LC-MS on a Thermo Scientific LTQ XL equipped with a diode array detector and using a Zorbax C_{18} column (5 μm , 80 \AA , 0.5×150 mm, Agilent Technologies). The analysis method (15 $\mu\text{L}/\text{min}$ flow rate) involved 15 mM aqueous NH_4OAc containing 2% CH_3CN followed by a linear gradient of 2–15% CH_3CN (0–15 min) and 25–60% CH_3CN (15–25 min). Wavelengths monitored = 260 nm. The concentration of the **DNA8-Abasic** species present after irradiation was determined by fitting the **DNA8/DNA7** ratios from each sample into the slope-intercept equation from the calibration plot to yield the amount of decoy (pmol) in the sample. This process was repeated from each prominent molecular ion observed in the photolysis sample. Furthermore, this quantitative analysis method assumes comparable ionization properties for the photolyzed products in comparison to the non-irradiated sample. First-order decay analysis (GraphPad Prism, v9.3.1) was performed with the data (percentage of starting material over time) to obtain the half-life ($t_{1/2}$) of the DNA decoy. Mean $t_{1/2}$ values (with standard deviation) were calculated from the fitting of the decay curve with the individual data points obtained from each replicate ($n=3$). To ensure that photolysis is not occurring on the non-modified base-pair (**DNA2**), the percentage of oligonucleotide remaining was analyzed from samples at $t=0$ to 25 min (Figure S8C). One-way ANOVA analysis (GraphPad Prism, v9.3.1) was performed with the data (percentage of oligonucleotide over photolysis time) and confirmed that there was no significant change in oligonucleotide remaining over time. Finally, LC-MS analysis of our decoy revealed the formation of the abasic lactone (m/z calcd: 4409.876; m/z found: 4411.0), which was monitored by changes observed in the UV absorbance (Figure S8D) as well as changes in the observed mass (Figure S8E). The slow formation of β - and δ -elimination products were also observed. The formed elimination products were similarly observed with the previously reported **7-NI** purine mimic.^[20]

Characterizing secondary structure of oligos by circular dichroism spectroscopy: CD spectroscopy was performed on a JASCO J-815 spectropolarimeter using previously described methods.^[48] Briefly, 15 nmol of DNA was annealed in PBS buffer. After annealing, prepared samples were placed into a 1 mm path length quartz cuvette (Starna cells cat# 21-Q-1) diluting to a total volume of 200 μL with additional PBS. Each sample was run two times and their spectra was averaged (Figure S9).

Light intensity determination: The intensity of the light source [I, Eq. (1)] was determined by using $\text{K}_3[\text{Fe}(\text{C}_2\text{O}_4)_3]$ actinometry as previously described for both the 254- and 350-nm bulbs.^[49,50]

$$I(\text{ein cm}^{-2} \text{s}^{-1}) = \frac{V_1 \times V_3 \times \Delta A_{510}}{1000 \left(\frac{\text{mL}}{\text{L}}\right) \times \epsilon_{510} \times V_2 \times \Phi_{\text{Fe}} \times t} \quad (1)$$

where V_1 is the volume of $\text{K}_3[\text{Fe}(\text{C}_2\text{O}_4)_3]$ irradiated (mL), V_2 is the volume of the $\text{K}_3[\text{Fe}(\text{C}_2\text{O}_4)_3]$ solution transferred to the volumetric flask (mL), V_3 is the volume of the volumetric flask (mL), ΔA_{510} is the difference in the absorbance at 510 nm between the irradiated and non-irradiated samples, ϵ_{510} is the extinction coefficient of $\text{K}_3[\text{Fe}(\text{C}_2\text{O}_4)_3]$ at 510 nm ($11100 \text{ M}^{-1} \text{cm}^{-1}$), Φ_{Fe} is the quantum yield of $\text{K}_3[\text{Fe}(\text{C}_2\text{O}_4)_3] \cdot 3\text{H}_2\text{O}$ (1.21), and t is the time irradiated (s). The intensity of the 254- and 350-nm bulbs was calculated and shown in Table S2.

Acknowledgements

We gratefully acknowledge the NIH (R01-GM110129) and the University of Minnesota for financial support. Mass spectrometry was performed at the University of Minnesota Masonic Cancer Center Analytical Biochemistry Core Facility, which is supported by the NIH (P30-CA77598). NMR spectrometry was performed at the University of Minnesota NMR Center.

Conflict of Interest

The authors declare no conflict of interest.

Data Availability Statement

The data that support the findings of this study are available in the supplementary material of this article.

Keywords: DNA decoys · DNA hybridization · nucleosides · oligonucleotides · photolysis

- [1] G. Mayer, A. Heckel, *Angew. Chem. Int. Ed.* **2006**, *45*, 4900–4921; *Angew. Chem.* **2006**, *118*, 5020–5042.
- [2] A. Deiters, *ChemBioChem* **2010**, *11*, 47–53.
- [3] N. Ankenbruck, T. Courtney, Y. Naro, A. Deiters, *Angew. Chem. Int. Ed.* **2018**, *57*, 2768–2798; *Angew. Chem.* **2018**, *130*, 2816–2848.
- [4] A. Dussy, C. Meyer, E. Quennet, T. A. Bickle, B. Giese, A. Marx, *ChemBioChem* **2002**, *3*, 54–60.
- [5] H. Lusic, M. O. Lively, A. Deiters, *Mol. BioSyst.* **2008**, *4*, 508–511.
- [6] M. Buff, T. Mack, A. Heckel, *Chimia* **2009**, *63*, 261–264.
- [7] J. M. Govan, M. O. Lively, A. Deiters, *J. Am. Chem. Soc.* **2011**, *133*, 13176–13182.
- [8] C. Menge, A. Heckel, *Org. Lett.* **2011**, *13*, 4620–4623.
- [9] F. Huang, M. You, D. Han, Z. Xiong, H. Liang, W. Tan, *J. Am. Chem. Soc.* **2013**, *135*, 7967–7973.
- [10] J. M. Govan, D. D. Young, M. O. Lively, A. Deiters, *Tetrahedron Lett.* **2015**, *56*, 3639–3642.
- [11] C. Höbartner, S. K. Silverman, *Angew. Chem. Int. Ed.* **2005**, *44*, 7305–7309; *Angew. Chem.* **2005**, *117*, 7471–7475.
- [12] L. Kröck, A. Heckel, *Angew. Chem. Int. Ed.* **2005**, *44*, 471–473; *Angew. Chem.* **2005**, *117*, 475–477.
- [13] X. Tang, J. Swaminathan, A. M. Gewirtz, I. J. Dmochowski, *Nucleic Acids Res.* **2008**, *36*, 559–569.
- [14] D. D. Young, H. Lusic, M. O. Lively, J. A. Yoder, A. Deiters, *ChemBioChem* **2008**, *9*, 2937–2940.
- [15] S. Shah, P. K. Jain, A. Kala, D. Karunakaran, S. H. Friedman, *Nucleic Acids Res.* **2009**, *37*, 4508–4517.

- [16] D. D. Young, J. M. Govan, M. O. Lively, A. Deiters, *ChemBioChem* **2009**, *10*, 1612–1616.
- [17] M. C. Buff, F. Schäfer, B. Wulffen, J. Müller, B. Pötzsch, A. Heckel, G. Mayer, *Nucleic Acids Res.* **2010**, *38*, 2111–2118.
- [18] D. D. Young, M. O. Lively, A. Deiters, *J. Am. Chem. Soc.* **2010**, *132*, 6183–6193.
- [19] S. M. A. H. Rad, L. Langroudi, F. Kouhkan, L. Yazdani, A. N. Koupaei, S. Asgharpour, Z. Shojaei, T. Bamdad, E. Arefian, *Tumor Biol.* **2015**, *36*, 4871–4881.
- [20] N. B. Struntz, D. A. Harki, *ACS Chem. Biol.* **2016**, *11*, 1631–1638.
- [21] L. Farahmand, B. Darvishi, A. K. Majidzadeh, *Drug Deliv.* **2017**, *24*, 1249–1261.
- [22] M. Hecker, A. H. Wagner, *Biochem. Pharmacol.* **2017**, *144*, 29–34.
- [23] M. M. Tehran, S. Rezaei, A. Jalili, S. H. Aghae-Bakhtiari, A. Sahebkar, *Drug Discovery Today* **2020**, *25*, 195–200.
- [24] J. L. Richards, X. Tang, A. Turetsky, I. J. Dmochowski, *Bioorg. Med. Chem. Lett.* **2008**, *18*, 6255–6258.
- [25] J. L. Richards, G. K. Sowards, Y.–H. Wang, I. J. Dmochowski, *ChemBioChem* **2010**, *11*, 320–324.
- [26] J. M. Govan, R. Uprety, J. Hemphill, M. O. Lively, A. Deiters, *ACS Chem. Biol.* **2012**, *7*, 1247–1256.
- [27] M. Kotera, A. G. Bourdat, E. Defrancq, J. Lhomme, *J. Am. Chem. Soc.* **1998**, *120*, 11810–11811.
- [28] M. Kotera, Y. Roupioz, E. Defrancq, A. G. Bourdat, J. Garcia, C. Coulombeau, J. Lhomme, *Chem. Eur. J.* **2000**, *6*, 4163–4169.
- [29] C. Crey-Desbiolles, N. Berthet, M. Kotera, P. Dumy, *Nucleic Acids Res.* **2005**, *33*, 1532–1543.
- [30] D. Loakes, D. M. Brown, *Nucleic Acids Res.* **1994**, *22*, 4039–4043.
- [31] R. Nichols, P. C. Andrews, P. Zhang, D. E. Bergstrom, *Nature* **1994**, *369*, 492–493.
- [32] A. V. Aerschot, J. Rozensky, D. Loakes, N. Pillet, G. Schepers, P. Herdewijn, *Nucleic Acids Res.* **1995**, *23*, 4363–4370.
- [33] D. E. Bergstrom, P. Zhang, P. H. Toma, P. C. Andrews, R. Nichols, *J. Am. Chem. Soc.* **1995**, *117*, 1201–1209.
- [34] D. Loakes, D. M. Brown, S. Linde, F. Hill, *Nucleic Acids Res.* **1995**, *23*, 2361–2366.
- [35] O. Amosova, J. Georg, J. R. Fresco, *Nucleic Acids Res.* **1997**, *25*, 1930–1934.
- [36] J. S. Oliver, K. A. Parker, J. W. Suggs, *Org. Lett.* **2001**, *3*, 1977–1980.
- [37] I. Hirao, T. Mitsui, M. Kimoto, S. Yokoyama, *J. Am. Chem. Soc.* **2007**, *129*, 15549–15555.
- [38] Z. Casar, I. Leban, A. M.-L. Maréchal, D. Lorcy, *J. Chem. Soc. Perkin Trans. 1* **2002**, 1568–1573.
- [39] M. Minuth, C. Richert, *Angew. Chem. Int. Ed.* **2013**, *52*, 10874–10877; *Angew. Chem.* **2013**, *125*, 11074–11077.
- [40] H. J. Lenox, C. P. McCoy, T. L. Sheppard, *Org. Lett.* **2001**, *3*, 2415–2418.
- [41] Y. Roupioz, J. Lhomme, M. Kotera, *J. Am. Chem. Soc.* **2002**, *124*, 9129–9135.
- [42] Y. Wang, T. L. Sheppard, S. Tornaletti, L. S. Maeda, P. C. Hanawalt, *Chem. Res. Toxicol.* **2006**, *19*, 234–241.
- [43] H. Ando, T. Furuta, R. Y. Tsien, H. Okamoto, *Nat. Genet.* **2001**, *28*, 317–325.
- [44] C. M. Connelly, R. Uprety, J. Hemphill, A. Deiters, *Mol. BioSyst.* **2012**, *8*, 2987–2993.
- [45] L. Wu, F. Pei, J. Zhang, J. Wu, M. Feng, Y. Wang, H. Jin, L. Zhang, X. Tang, *Chem. Eur. J.* **2014**, *20*, 12114–12122.
- [46] M. J. Robins, R. K. Robins, *J. Am. Chem. Soc.* **1965**, *87*, 4934–4940.
- [47] P. C. Srivastava, R. K. Robbins, F. Takusagawa, H. M. Berman, *J. Heterocycl. Chem.* **1981**, *18*, 1659–1662.
- [48] K. T. Passow, D. A. Harki, *Org. Lett.* **2018**, *20*, 4310–4313.
- [49] J. N. Demas, W. D. Bowman, E. F. Zalewski, R. A. Velapoldi, *J. Phys. Chem.* **1981**, *85*, 2766–2771.
- [50] H. Kuhn, S. Braslavsky, R. Schmidt, *Pure Appl. Chem.* **1989**, *76*, 2105–2146.

Manuscript received: May 2, 2022

Accepted manuscript online: July 18, 2022

Version of record online: August 25, 2022